Chinese Journal of Aeronautics, (2014),27(6): 1430–1441

Chinese Society of Aeronautics and Astronautics
& Beihang University

Chinese Journal of Aeronautics

cja@buaa.edu.cn
www.sciencedirect.com

A new stress-based multi-scale failure criterion of composites and its validation in open hole tension tests

Li Xing, Guan Zhidong *, Li Zengshan, Liu Lu

School of Aeronautic Science and Engineering, Beihang University, Beijing 100191, China

Received 16 September 2013; revised 18 November 2013; accepted 10 February 2014
Available online 17 October 2014

KEYWORDS

Composite material;
Failure criterion;
Multi-scale;
Off-axis tension;
Open-hole tension

Abstract A new stress-based multi-scale failure criterion is proposed based on a series of off-axis tension tests, and their corresponding fiber failure modes and matrix failure modes are determined at the microscopic level. It is a physical mechanism based, three-dimensional damage analysis criterion which takes into consideration the constituent properties on the macroscopic failure behavior of the composite laminates. A complete set of stress transformation, damage determination and evolution methods are established to realize the application of the multi-scale method in failure analysis. Open-hole tension (OHT) specimens of three material systems (CCF300/5228, CCF300/5428 and T700/5428) are tested according to ASTM standard D5766, and good agreements are found between the experimental results and the numerical predictions. It is found that fiber strength is a key factor influencing the ultimate strength of the laminates, while matrix failure alleviates the stress concentration around the hole. Different matchings of fiber and matrix result in different failure modes as well as ultimate strengths.

© 2014 Production and hosting by Elsevier Ltd. on behalf of CSAA & BUAA.
Open access under CC BY-NC-ND license.

1. Introduction

Due to the high ratio of strength/stiffness to weight and good corrosion resistance, etc., fiber–reinforced composite materials are widely used in modern aero-plane structures. It has been demonstrated that primary aircraft structures made from carbon fiber composites can achieve weight savings of 20%–30% over similarly designed metal structures.[1] Airbus uses 25% composites in A380 structures and Boeing uses up to 50% in Boeing 787 structures, and the percentage of composite materials used in commercial jet aero-planes becomes a symbol of technology advantage and market competitiveness.[2] For its great importance to structure safety, failure behavior and strength prediction of composite materials have been reported extensively in the literature. After several decades of development, countless efforts have been made in this area, and substantial achievements have been obtained.[3] Some well-known failure criteria such as Tsai-Wu tensor criterion,[4] Hashin criterion,[5] etc. can effectively predict the failure strength of

* Corresponding author. Tel.: +86 10 82317538.
E-mail addresses: lixingd506@163.com (X. Li), zdguan@buaa.edu.cn (Z. Guan).

Peer review under responsibility of Editorial Committee of CJA.

ELSEVIER Production and hosting by Elsevier

http://dx.doi.org/10.1016/j.cja.2014.10.009
1000-9361 © 2014 Production and hosting by Elsevier Ltd. on behalf of CSAA & BUAA. Open access under CC BY-NC-ND license.

composites and have been widely used in engineering practice. The world-wide failure exercise (WWFE) sponsored by Hinton et al.[6] provides a good opportunity for comparison of all the participant failure theories against experimental results, and comprehensive assessment of 19 leading failure theories was presented, including their validities and shortfalls. All theories were ranked according to their abilities to predict a wide range of experimental results.

However, conventional failure models are almost phenomenological and rely on a number of parameters fitted with experimental results, whose physical meanings are not always well established.[7] They usually treat the fiber–matrix system as a whole and determine failure at the ply level, which can hardly distinguish whether failure occurs in fiber, matrix, or at fiber–matrix interface, even though some efforts have been made. In order to establish the link between the properties of composite constituents (fiber, matrix and interface) and macroscopic performance, the Accelerated Insertion of Materials-Composite Program (AIM-C) devised by Defense Advanced Research Projects Agency (DARPA) in 2001 suggested to develop physical mechanism based analysis methods and multi-scale failure models, which allow the designer to reliably predict damage and its growth down to the micromechanic level for a given design option, while simultaneously incorporating material and processing variability.[8]

In such a context, some failure theories based on micromechanics were developed. Gosse and Christensen[9] proposed strain invariant failure theory (SIFT) in 2001, which identifies fiber and matrix failure by two strain invariants in the micro-level, and attributes matrix failure to dilatation as well as distortion failure. The multi-continuum theory (MCT) by Mayes and Hansen,[10,11] in which the constitutive equations of fiber and matrix are formulated by stresses at a point, identifies their failures by quadratic stress failure criteria respectively. In Wang's theory,[12] the improved von Mises yield criterion is adopted to judge matrix failure, while the micro-buckling failure mode of fiber under compression is captured. Considering the failure of fiber, matrix and interface, the micro-mechanics of failure (MMF) criterion proposed by Ha et al.[13,14] formulates damage determination and evolution methods. Bednarcyk et al.[15,16] uses a micromechanics model called the generalized method of cells to evaluate failure criteria at the micro-level, and a corresponding analysis platform FEAMAC is presented. Gotsis et al.[17] and Huang[18] have also proposed other micromechanics-based failure criteria respectively. Up to now, multi-scale failure criteria have been used in fracture and durability analyses of composite structures,[19–22] and these criteria also make use of the analysis of residual thermal stresses and fiber volume fraction's effects on the mechanical behaviors of composite laminates.[23–25]

Meanwhile, the multi-scale failure analysis methods still require considerable improvements. For example, the SIFT criterion can only predict damage initiation while the MMF criterion always underestimates the shear strength of the laminate.[21] Problems such as the stress/strain transition between microscopic and macroscopic levels, and the determination and evolution of failure modes in micro-level, also need to be further investigated. Intending to solve the problems mentioned above, this paper proposes a new stress-based multi-scale failure model based on experimental observations, and the failure behaviors of fiber and matrix at microscopic level are properly defined. Square and hexagon representative volume elements (RVEs) are introduced to transform macroscopic stresses to microscopic stresses, and the corresponding damage evolution methods are established. In order to validate the multi-scale failure criterion, open-hole tension performance of three material systems (CCF300/5228, CCF300/5428, and T700/5428) are tested, and numerical models based on this failure theory are used to analyze the effect of constituent properties on the open-hole tension performance of carbon fiber reinforced plastics (CFRP) laminates.

2. Proposal of multi-scale failure model of composites

2.1. Transformation from macro stresses to micro stresses

As the average value between fiber and matrix, macroscopic stresses obtained by mechanical experiments in laminates can't describe the actual stress distribution in the microscopic level. However, under the arrangement assumption of fiber and matrix, stresses applied on the laminate can be equivalently transformed to the stresses applied on the RVE, as shown in Fig. 1. Therefore, microscopic stresses in fiber and matrix can be obtained by FE analysis on RVEs, which can be written using stress amplification factors:

$$\boldsymbol{\sigma} = \boldsymbol{M}_{\sigma}\bar{\boldsymbol{\sigma}} + \boldsymbol{A}_{\sigma}\Delta T \tag{1}$$

where $\boldsymbol{\sigma}$ and $\bar{\boldsymbol{\sigma}}$ (6×1) are the microscopic and macroscopic stress vectors respectively, $\boldsymbol{M}_{\sigma}$ (6×6) is the matrix of mechanical stress amplification factors caused by different mechanical properties of fiber and matrix, and $\boldsymbol{A}_{\sigma}$ (6×1) is the matrix of thermal stress amplification factors caused by their different thermal expansion coefficients.

Fig. 2 is the representative distributions of fiber and matrix considered in this paper. Square and hexagon RVEs are used to obtain stress amplification factors, where 1 describes fiber direction and 2, 3 the normal directions of the fiber. A set of reference points in the RVEs is chosen to analyze the stresses in fiber and matrix respectively. Due to the symmetrical stress distribution in the RVEs, all reference points are in the upper side of the model. The reference points chosen are the maximum stress points under different loading cases, which can cover the dangerous points in calculation. In the square RVE, 6 out of 16 reference points (F1–F6) are in the fiber and the other 10 (M1–M10) are in the matrix, while in the hexagon RVE, 8 out of 21 reference points (F1–F8) are in the fiber and the other 13 (M1–M13) are in the matrix. Mechanical and thermal stress amplification factors are calculated at each reference point of the RVEs. The relationship between macro stresses and micro stresses can be expressed as

$$\begin{bmatrix}\sigma_1\\ \sigma_2\\ \sigma_3\\ \sigma_{12}\\ \sigma_{13}\\ \sigma_{23}\end{bmatrix} = \begin{bmatrix}M_{11} & M_{12} & M_{13} & M_{14} & M_{15} & M_{16}\\ M_{21} & M_{22} & M_{23} & M_{24} & M_{25} & M_{26}\\ M_{31} & M_{32} & M_{33} & M_{34} & M_{35} & M_{36}\\ M_{41} & M_{42} & M_{43} & M_{44} & M_{45} & M_{46}\\ M_{51} & M_{52} & M_{53} & M_{54} & M_{55} & M_{56}\\ M_{61} & M_{62} & M_{63} & M_{64} & M_{65} & M_{66}\end{bmatrix}\begin{bmatrix}\bar{\sigma}_1\\ \bar{\sigma}_2\\ \bar{\sigma}_3\\ \bar{\sigma}_{12}\\ \bar{\sigma}_{13}\\ \bar{\sigma}_{23}\end{bmatrix} + \begin{bmatrix}A_{11}\\ A_{21}\\ A_{31}\\ A_{41}\\ A_{51}\\ A_{61}\end{bmatrix}\Delta T \tag{2}$$

In the aspect of $\boldsymbol{M}_{\sigma}$ calculation, normalized stresses are applied on the boundaries of the RVEs by nodes coupled with each face, seen in Fig. 3. When $\bar{\boldsymbol{\sigma}}_1$ is applied, micro stresses at each reference point can be obtained, and the first column of

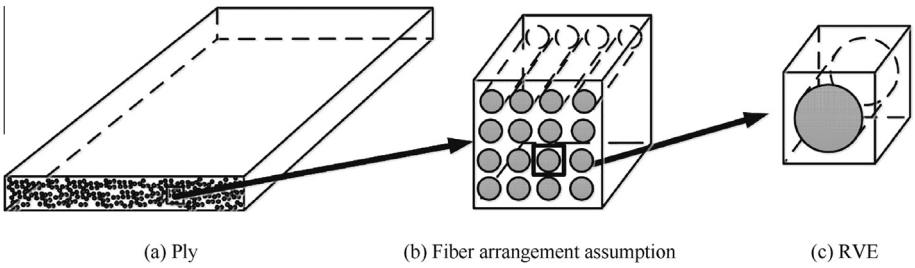

Fig. 1 Composite macro–micro transition.

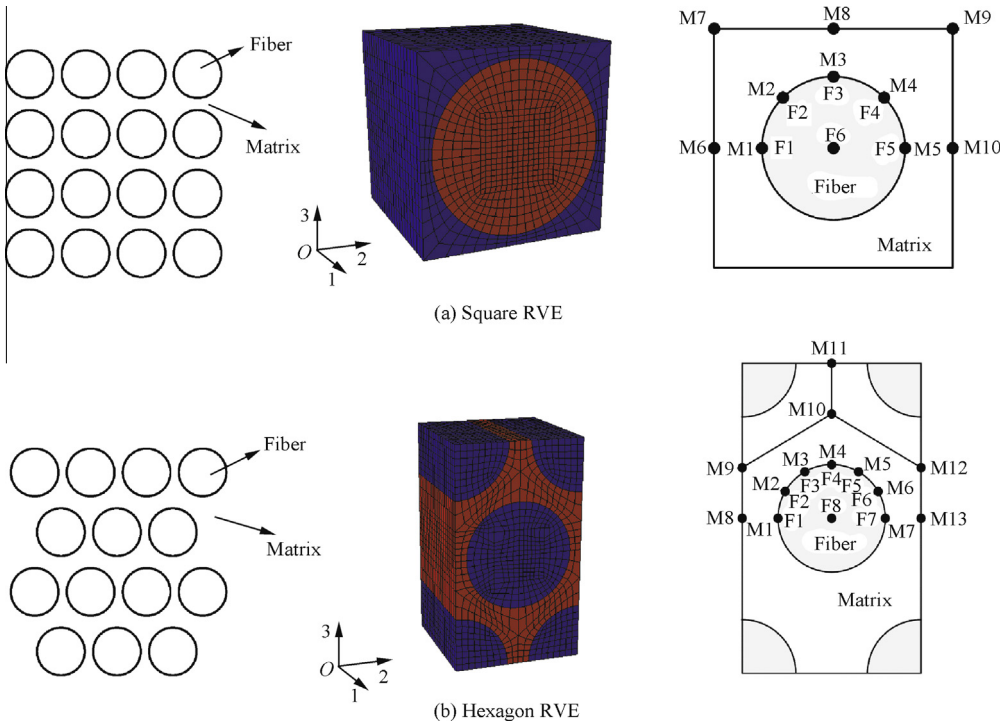

Fig. 2 RVE determination and reference points chosen.

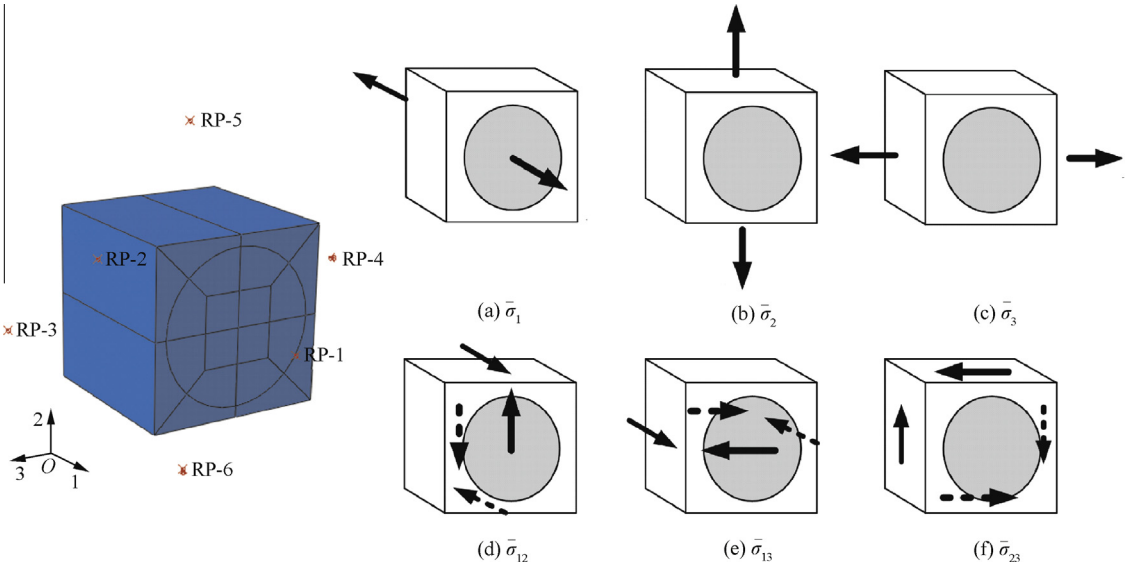

Fig. 3 Macro stresses applied on boundary of RVEs in calculation of $\boldsymbol{M}_{\sigma}$.

$\boldsymbol{M}_{\sigma}$ is calculated. The other columns of $\boldsymbol{M}_{\sigma}$ can be calculated in the same way. In the aspect of $\boldsymbol{A}_{\sigma}$ calculation, the boundaries of the RVEs are constrained and a temperature increment is applied, and then $\boldsymbol{A}_{\sigma}$ can be obtained by the corresponding micro stresses.

In damage determination and evolution, both square and hexagon RVEs will be considered. It is noted that the loading direction may not be the same as the assumed fiber arrangement, so rotation of the RVEs around axis 1 is also considered, seen in Fig. 4. The corresponding stresses in the unit cell axes (1, 2 and 3) can be calculated from the loading directions (1′, 2′ and 3′) by

$$\begin{bmatrix}\sigma_1\\ \sigma_2\\ \sigma_3\\ \sigma_{12}\\ \sigma_{13}\\ \sigma_{23}\end{bmatrix}=\begin{bmatrix}1 & 0 & 0 & 0 & 0 & 0\\ 0 & \cos^2\alpha & \sin^2\alpha & 0 & 0 & 2\sin\alpha\cos\alpha\\ 0 & \sin^2\alpha & \cos\alpha & 0 & 0 & -2\sin\alpha\cos\alpha\\ 0 & 0 & 0 & \cos\alpha & \sin\alpha & 0\\ 0 & 0 & 0 & -\sin\alpha & \cos\alpha & 0\\ 0 & -\sin\alpha\cos\alpha & \sin\alpha\cos\alpha & 0 & 0 & \cos^2\alpha-\sin^2\alpha\end{bmatrix}\begin{bmatrix}\sigma'_1\\ \sigma'_2\\ \sigma'_3\\ \sigma'_{12}\\ \sigma'_{13}\\ \sigma'_{23}\end{bmatrix} \tag{3}$$

2.2. Characterization of microscopic failure modes

Unlike traditional metal materials, composites are made up of two constituents with a large mismatch in mechanical and thermal properties, in which failure can be distinguished in fiber, matrix or interface depending on the loading conditions. Fiber behaves highly anisotropic in the composite, whose stiffness and strength are far beyond the matrix. When loaded in the fiber's direction, stresses in the composite are mainly undertaken by the fibers, which can be considered as fiber-controlled loading condition, and the corresponding failure modes are divided into fiber tensile failure and compressive failure.

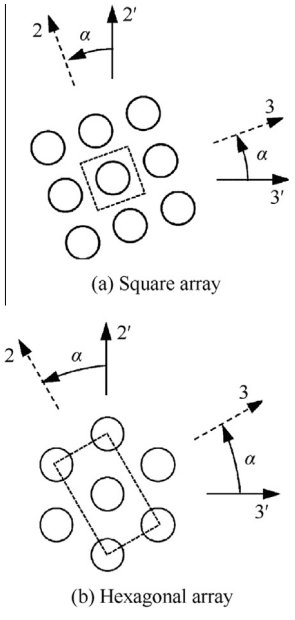

Fig. 4 RVE rotation with respect to loading direction.[13]

Gosse and Christensen[9] employs the von Mises strain which is related to the second deviatoric strain invariant to define fiber failure in SIFT, while Wang[12] takes into account micro-buckling effect when compressive loaded is applied. Since fiber always shows brittle fracture in composite laminates, which can be seen as the intrinsic property of fiber, it is rational to use the maximum stress failure criterion to define fiber failure:

(1) Fiber tensile failure

$$\sigma_{f1} > X_{ft}, \quad \sigma_{f1} > 0 \tag{4}$$

(2) Fiber compressive failure

$$\sigma_{f1} < -X_{fc}, \quad \sigma_{f1} \leqslant 0 \tag{5}$$

where σ_{f1} is the longitudinal stress of the fiber, and X_{ft} and X_{fc} are the longitudinal tensile and compressive strengths of the fiber, respectively.

The main controversial issue is the definition of matrix failure, as well as the failure of fiber/matrix interface. Many articles have discussed the influence of matrix and interface properties on the performance of the laminates,[26–29] Ha et al.[13] distinguish matrix failure and interface failure in MMF failure theory. However, many hypotheses have to be made since it is difficult to precisely characterize matrix failure and interface failure respectively. On the other hand, for a composite material system in practical use, the fiber sizing should be carefully determined and interface failure should not be a dominant factor. Therefore, only matrix failure is considered in this paper for the purpose of simplification and practical application.

In most cases, bulk matrix materials can be seen as isotropic and plastic displaying different yield stresses in tension and compression, which is attributed to the effect of hydrostatic stress on shear-driven yielding. The classical yield criteria, e.g., von Mises and Tresca criteria have thus been modified to account for sensitivity to the hydrostatic stresses.[30] The modified criteria fit well with experimental results for bulk polymers in yielding, while the in-situ performance of the matrix in composites may not be the same. Asp et al.[31] find that when matrix is constrained between fibers, yielding is suppressed while brittle failure occurs, which is presumably caused by crack growth from cavitation. Cavitation characterization and failure envelope for matrix in composites are shown in Fig. 5.[31,32] It can be seen that there is a truncation in the first quadrant of the matrix failure envelope (tension–tension loading), which represents the failure mechanism caused by cavitation. In the other three quadrants, the matrix failure is still controlled by yielding. So two failure mechanisms of matrix should be defined: dilatational failure caused by

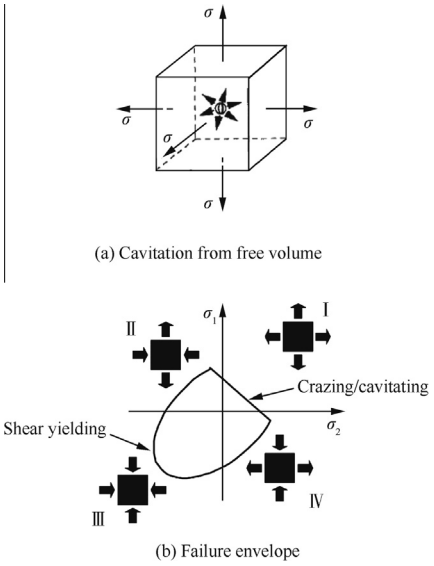

Fig. 5 Cavitation from free volume and failure envelope for matrix in composites.[31,32]

cavitation, and distortional failure caused by yielding. In SIFT[9] volumetric strain and equivalent strain are used to identify these two failure modes, the strain invariants are

$$\begin{cases} J_1 = \varepsilon_{xx} + \varepsilon_{yy} + \varepsilon_{zz} \\ J_2' = \dfrac{1}{6}\left[(\varepsilon_{xx} - \varepsilon_{yy})^2 + (\varepsilon_{yy} - \varepsilon_{zz})^2 + (\varepsilon_{xx} - \varepsilon_{zz})^2\right] \\ + \dfrac{1}{4}\left(\gamma_{xy}^2 + \gamma_{yz}^2 + \gamma_{xz}^2\right) \varepsilon_{\mathrm{VM}} = \sqrt{3J_2'} \end{cases} \tag{6}$$

where J_1 is the first strain invariant, i.e., the volumetric strain, J_2' is the second deviatoric strain invariant, i.e., the equivalent strain, and $\varepsilon_{\mathrm{VM}}$ is the von Mises strain related to J_2'. SIFT employs J_1 and $\varepsilon_{\mathrm{VM}}$ to characterize the above two failure modes, ε_{ij} $(i, j = x, y, z)$ are the strain component.

In this paper the dilatational and distortional failure modes of matrix are also recognized, while stress invariants are used to identify failure. Strain variables are replaced because composite strengths expressed by stresses are more universal and easier to obtain, and it is more convenient to define damage evolution by stresses. Similarly, two stress invariants I_1 and σ_{VM} are introduced by

$$\begin{cases} I_1 = \sigma_{xx} + \sigma_{yy} + \sigma_{zz} \\ I_2 = \sigma_{xx}\sigma_{yy} + \sigma_{yy}\sigma_{zz} + \sigma_{xx}\sigma_{zz} - (\tau_{xy}^2 + \tau_{xz}^2 + \tau_{yz}^2) \\ \sigma_{\mathrm{VM}} = \sqrt{I_1^2 - 3I_2} \end{cases} \tag{7}$$

where I_1 is the volumetric stress invariant, i.e., the first stress invariant, and σ_{VM} is the deviatoric stress invariant, i.e., von Mises equivalent stress.

Based on the above mentioned research findings, this paper intends to further characterize the in-situ failure behavior of the matrix in composites, so off-axis tensile tests of 10°, 30°, 45°, 67°and 90° unidirectional stacked laminates are conducted with three composite systems (CCF300/5228, CCF300/5428 and T700/5428), whose strengths are shown in Table 1. Take CCF300/5428 as an example, the stresses in the material axis can be obtained from an off-axis laminar (seen in Fig. 6) by

$$\begin{cases} \sigma_1 = \sigma_x \cos^2\theta \\ \sigma_2 = \sigma_x \sin^2\theta \\ \tau_{12} = -\sigma_x \sin\theta\cos\theta \end{cases} \tag{8}$$

where σ_1, σ_2 and τ_{12} are stresses in the material axis, σ_x is the off-axis loading stress, and θ is the angle between the fiber and the loading direction. Take the off-axis ultimate strength σ_{xu} into Eq. (6) and the corresponding σ_{1u}, σ_{2u} and τ_{12u} can be obtained, which are applied as boundary stresses of the RVEs in Fig. 2. The stresses in every reference point of the RVEs are calculated, and the corresponding I_1 and σ_{VM} can be obtained, which are all shown in the failure loci of σ_{VM}—I_1 plane, as seen in Fig. 7.

From the σ_{VM}—; I_1 failure loci, we can see the ultimate von Mises equivalent stresses (representing yielding failure) of the off-axis tests differ greatly. For example the maximum σ_{VM} in 10° tension is about two times larger than the maximum σ_{VM} in 90° tension. Meanwhile, the maximum I_1 (representing cavitation growth failure) in 90° tension is much larger than in 10° tension. This demonstrates that the failure mechanism of matrix in composites is not all controlled by yielding, which is not the same as bulk resin, and this accords with the conclusion drawn by Asp et al. mentioned above. So we also define two failure modes of the matrix, dilatational failure controlled by cavitation growth and distortional failure controlled by yielding. In the 90° unidirectional tension test, I_1 of the matrix achieves the maximum value and its corresponding σ_{VM} is nearly zero, which can be used to obtain the critical first stress invariant $I_{1-\mathrm{crit}}$ and define the dilatational failure of the matrix. In 10° unidirectional tension test, the matrix fails in distortion,[33] so we use it to obtain the critical von Mises equivalent stress $\sigma_{\mathrm{VM-crit}}$ and define distortional failure of the matrix.

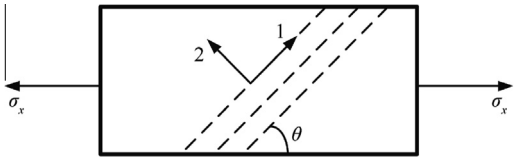

Fig. 6 Transformation from off-axis coordinates to material coordinates.

Table 1 Strength of three material systems.

Material type	Strength (MPa)								
	0° tensile	10° tensile	30° tensile	45° tensile	67° tensile	90° tensile	0° compressive	90° compressive	Shear
CCF300/5228	1744	687	198	135	93	81	−1230	245	120
CCF300/5428	1858	584	169	102	73	69	−1318	229	102
T700/5428	2450	550	173	92	71	65	−1210	220	111

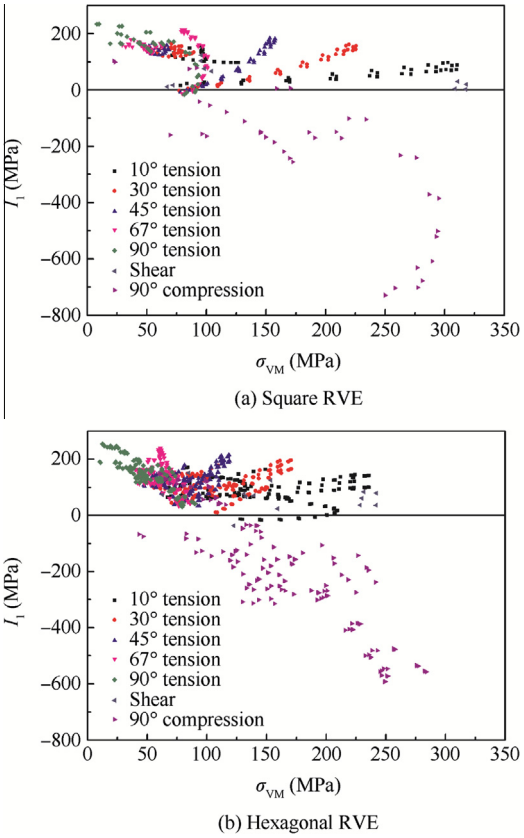

Fig. 7 Distribution of micro stress invariants in matrix of square and hexagonal RVEs (CCF300/5428).

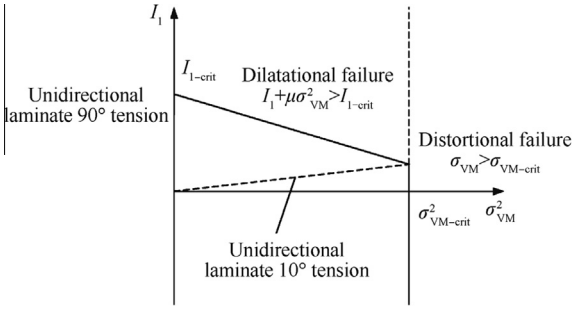

Fig. 8 Failure envelope of matrix.

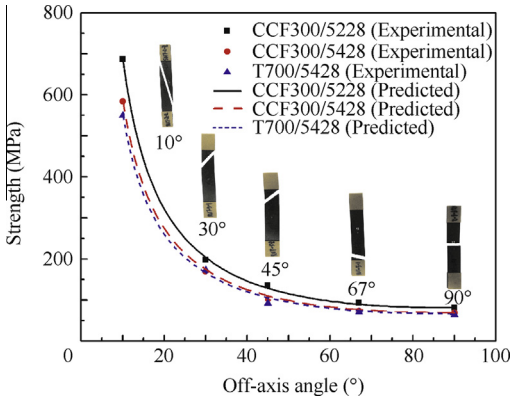

Fig. 9 Overall failure of off-axis laminates and theoretical predictions.

However, there is an obvious deviation between 90°, 30° and 45° tensile results, so a correlation factor μ denoting the influence of deviatoric stress on dilatational failure of matrix is introduced. Matrix failure can thus be defined as:

(3) Matrix dilatational failure

$$I_1 + \mu\sigma^2_{VM} > I_{1-crit} \tag{9}$$

(4) Matrix distortional failure

$$\sigma_{VM} > \sigma_{VM-crit} \tag{10}$$

Critical values of multi-scale failure criterion, i.e., X_{ft}, X_{fc}, I_{1-crit}, $\sigma_{VM-crit}$ and μ can be obtained from the corresponding experiments shown in Table 2, and Fig. 8 is the failure envelope of the matrix as well as the definition of the two failure modes. The theoretical predictions using this new failure model are compared with off-axis experimental results in Fig. 9, which shows good agreements between experiments and predictions.

2.3. Damage determination and evolution

The procedures of damage determination and evolution by the multi-scale failure criterion in finite element (FE) simulation are shown in Fig. 10. After macro stresses $\bar{\boldsymbol{\sigma}}$ of each element are obtained, micro stresses are calculated from macro stresses using Eq. (1) at every reference point of the square and hexagon RVE models. Then whether damage occurs is checked by the failure criteria of fiber or matrix in Eqs. (4), (5), (9), (10). If damage does not appear, the calculation will go to the next iteration directly. If any reference point of the RVEs in the fiber

Table 2 Failure modes and critical values determination.

Failure mode	Critical value	Corresponding experiment
Fiber tension	Fiber tensile strength X_{ft}	Unidirectional laminate 0° tension
Fiber compression	Fiber compressive strength X_{fc}	Unidirectional laminate 0° compression
Matrix dilatation	Matrix critical first stress invariant I_{1-crit}	Unidirectional laminate 90° tension
	Correlation factor μ	Unidirectional laminate 10° tension
Matrix distortion	Matrix critical von Mises stress $\sigma_{VM-crit}$	Unidirectional laminate 10° tension

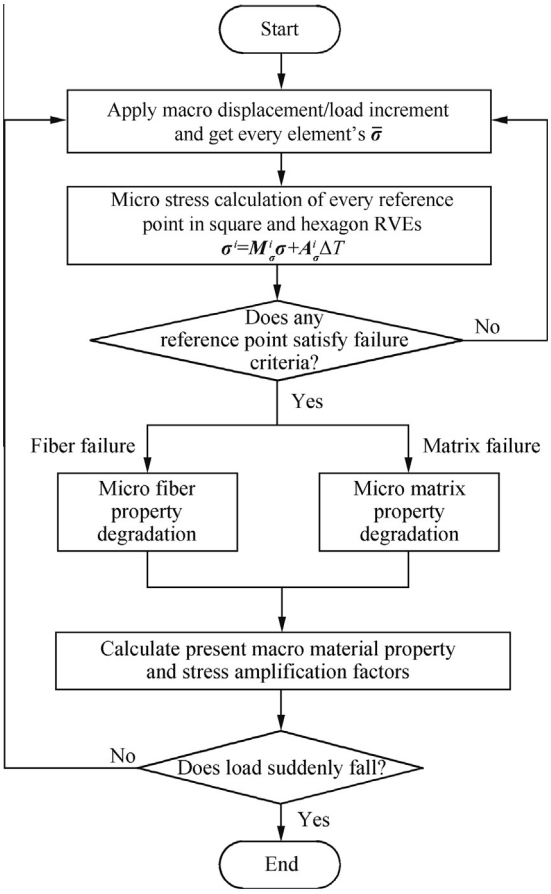

Fig. 10 Flowchart for damage determination and evolution.

satisfies the micro fiber failure criterion, then macro properties of the element should be degraded, so that the matrix failure occurs, and then a new iteration will be executed. The FE analysis will be finished once a sharp decrease of load occurs.

In damage determination of the reference points, fiber failure should only be examined in the reference points located in the fiber of the RVEs, and matrix failure should be examined in the reference points located in the matrix. According to different failure modes, the macro properties of the laminar should be degraded through the calculation in the RVE models. For example, when fiber failure occurs, the longitudinal modulus of the fiber in RVE is degraded, and the degraded modulus of the RVE can be calculated. Corresponding procedure will be carried out when failures happen to matrix. The degradation coefficients of fiber and matrix are defined as:

(1) Fiber failure

$$\begin{cases} E_1^* = 0.001E_1, \quad E_2^* = E_2, \quad E_3^* = E_3 \\ v_{12}^* = 0.1v_{12}, \quad v_{13}^* = 0.1v_{13}, \quad v_{23}^* = v_{23} \\ G_{12}^* = 0.1G_{12}, \quad G_{13}^* = 0.1G_{13}, \quad G_{23}^* = G_{23} \end{cases} \tag{11}$$

where the symbols on the left side of the equations represent the degraded macro properties, while the symbols on the right side of the equations represent the original macro properties of composites.

(2) Matrix failure

$$E^* = 0.1E, \quad v^* = v \tag{12}$$

Which are determined to be best fitted with experimental results. Meanwhile, stress amplification factors should also be regenerated according to the degradation of the RVE models. The summary of failure determination and material property degradation is listed in Table 3.

3. Experiment validation

3.1. Material and experiment procedure

To validate the proposed multi-scale failure criterion, open-hole tension (OHT) performance of three CFRP material systems are studied, which are CCF300/5228, CCF300/5428 and T700/5428. CCF300 is a kind of carbon fiber manufactured by Guangwei Group of China, which has properties equivalent to T300 made by Toray Company, and T700 is made by Toray Company of Japan. 5228 is a toughened thermoset epoxy resin while 5428 is a toughened bismaleimide resin, all of which are manufactured by Beijing Aeronautic Material Academe of AVIC (Aviation Industry Corporation of China). The specimen preparation and test procedure are based on ASTM Standard D5766.[34] The specimen size is 250 mm × 36 mm and d/W ratio is 1/6, where d is the hole diameter and W is the aminate width. The laminates are quasi-isotropic stacked of $[45/0/-45/90]_{3s}$ and the thickness of an individual ply is

Table 3 Damage determination and material property degradation.

Failure mode	Reference point	Failure criteria	Micro property degradation
Fiber tension	F1–F6 (Square) F1–F8 (Hexagon)	$\sigma_{fl} > X_{ft}$	Fiber
Fiber compression	F1–F6 (Square) F1–F8 (Hexagon)	$\sigma_{fl} < -X_{fc}$	Fiber
Matrix expansion	M1–M10 (Square) M1–M13 (Hexagon)	$I_1 + \mu\sigma_{VM}^2 > I_{1-crit}$	Matrix
Matrix distortion	M1–M10 (Square) M1–M13 (Hexagon)	$\sigma_{VM} > \sigma_{VM-crit}$	Matrix

Note: σ_{fl} is fiber stress, X_{ft}, X_{fc} are respectively fiber's tensile strength and compressive strength, I_1 is the first stress invariant, σ_{VM} is von-Mises stress invariant, μ is correlation factor.

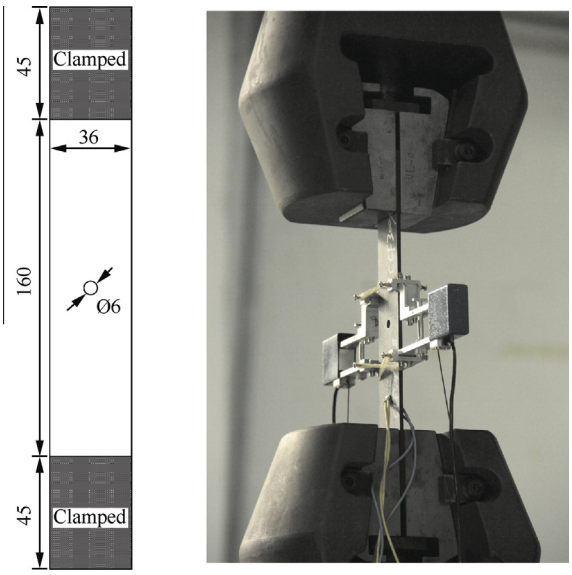

Fig. 11 Geometry of OHT specimen and experiment setting.

0.125 mm. All the test specimens are manufactured in autoclaves at Beijing Aeronautic Material Academe of AVIC.

Fig. 11 shows the geometry of the OHT specimens and the corresponding experiment setting. Experiments were conducted in a WDW-200E universal electronic testing machine made in Jinan of China, and three specimens for each material system were tested until failure to determine the average OHT strengths as well as the stress–strain curves. Both ends of the specimen were clamped in the grips using a sheet of sand paper to prevent slipping. After a 5 kN preload, tests were carried out at a constant cross-head speed of 1 mm/min while load and displacement were measured automatically by the computer.

3.2. Experiment results

Fig. 12 shows the fracture morphologies and C-scan results of OHT specimens for each of the material systems. The ultimate strength of CCF300/5228 (325 MPa) is not far from CCF300/5428 (375 MPa), and the difference is mainly caused by the performance of the matrix. T700/5428 has a much higher strength (517 MPa) than CCF300/5228 and CCF300/5428 laminates, which is attributed to the much higher

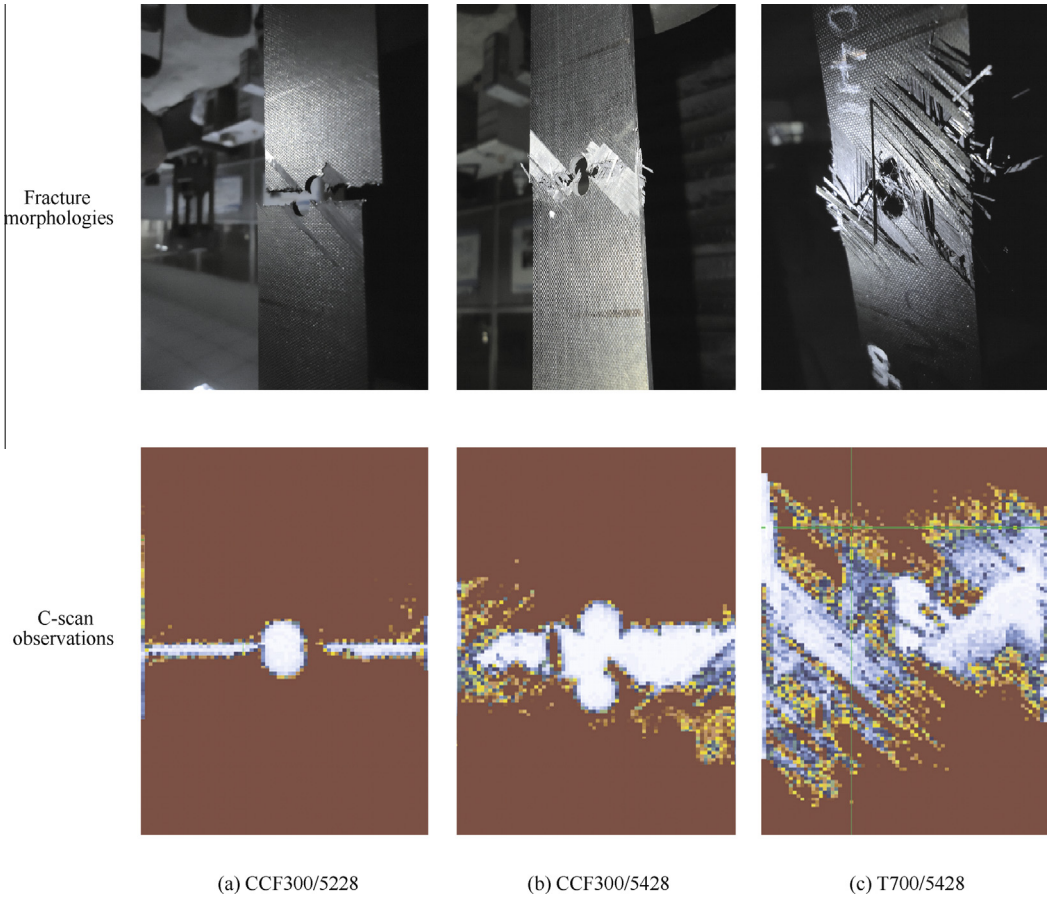

Fig. 12 Fracture morphologies and C-scan observations of OHT specimens.

strength of T700 fiber. From Fig. 12 we can see that the OHT specimens of CCF300/5228 failed in a brittle manner, with a fairly clean fracture perpendicular to the loading direction. While in specimens of CCF300/5428, more extensive damage occurred prior to failure with ply cracking across the entire width of the specimen, which was more evident in plies close to the surface. Moreover, T700/5428 showed considerable fiber pull-out and ply cracking at final failure. The C-scan observations also agreed with the above conclusions. Meanwhile, from the C-scan results we can see that delamination (shown in different colors from red) was almost limited in the regions of intra-laminar failure, so delamination was not the major failure mode in all the three types of quasi-orthotropic OHT laminates.

4. Numerical simulation and discussion

The experimental results above show that OHT performance of CFRP laminates is rather complex depending on different matches of fiber and matrix. In order to demonstrate the feasibility of the multi-scale failure criterion and to understand in-depth the role of constituent properties which play in OHT response, all the test cases are simulated using finite element software ABAQUS with secondarily developed subroutines of multi-scale failure analysis. Numerical results are compared with experimental results, and discussions are made in the following.

4.1. FE modeling of OHT laminates

The modeling strategy to simulate the OHT performance of quasi-isotropic laminates $[45/0/-45/90]_{3s}$ is depicted in Fig. 13. Because of the in-plane symmetry of the stacking sequence, one half of the specimen was modeled, applying symmetric boundary conditions in the middle plane. For computational efficiency, only the portion centered in the hole of the specimen was modeled, therefore the FE model size was 54 mm × 36 mm × 1.5 mm (each ply thickness was 0.125 mm). The radius of the centered hole was r = 6.0 mm. One side of the laminate was fixed and displacement was applied to a reference node coupled with the other side. The areas highlighted in Fig. 13 were intact without damage determination to prevent premature failure due to boundary effects. Multi-scale failure criterion was applied to plies of the remnant part to simulate progressive failure of the laminate.

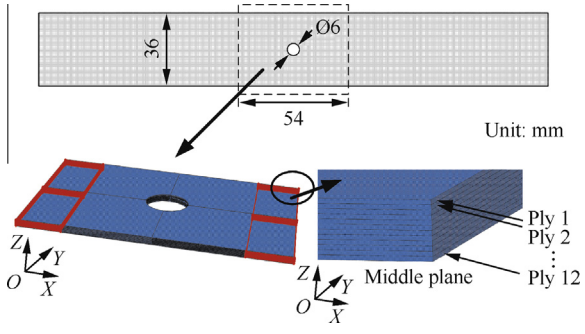

Fig. 13 Modeling strategy of OHT laminate.

Plies of the laminate were meshed using 3D liner solid elements, and there were totally 23016 linear hexahedral elements of type C3D8R. Material properties of three material systems were shown in Table 4.[35,36]

4.2. Numerical results and discussion

The ultimate strengths predicted by numerical simulations are compared with experimental results in Table 5, and Fig. 14 is the simulated stress–strain curves of three kinds of OHT specimens, all of which show good agreement with the experiment

Table 5 Comparison of simulated strength with experimental strength of OHT.

Material type	Experimental strength (MPa)	Simulated strength (MPa)	Error (%)
CCF300/5228	325	311	4.3
CCF300/5428	375	351	6.4
T700/5428	517	493	4.6

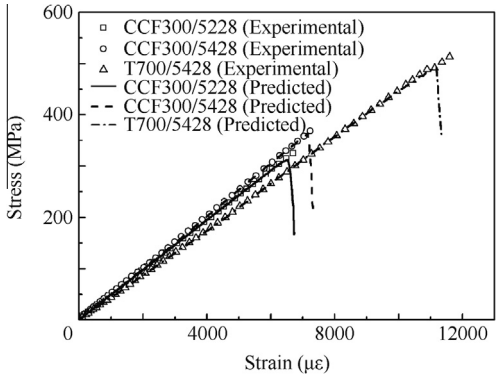

Fig. 14 Simulated stress–strain curves of OHTs.

Table 4 Material properties of UD laminate.[35,36]

Material type	V_f	E_1 (GPa)	$E_2 = E_3$ (GPa)	$G_{12} = G_{13}$ (GPa)	G_{23} (GPa)	$v_{12} = v_{13}$	v_{23}	α_1 (10^{-7}/°C)	α_2 (10^{-5}/°C)
CCF300/5228	0.63	137	8.80	4.40	6.43	0.320	0.46	1.50	3.54
CCF300/5428	0.63	145	9.75	5.69	5.69	0.312	0.44	4.00	2.50
T700/5428	0.63	125	7.80	5.60	5.70	0.320	0.46	9.70	2.09

Notes: V_f is fiber volume fraction, E_1 is longitudinal modulus, E_2 and E_3 are transverse modulus, G_{12} and G_{13} are in-plane shear modulus, G_{23} is transverse shear modulus, v_{12} and v_{13} are in-plane Poisson's ratio, v_{23} is transverse Poisson's ratio, α_1 and α_2 are longitudinal and transverse thermal coefficients.

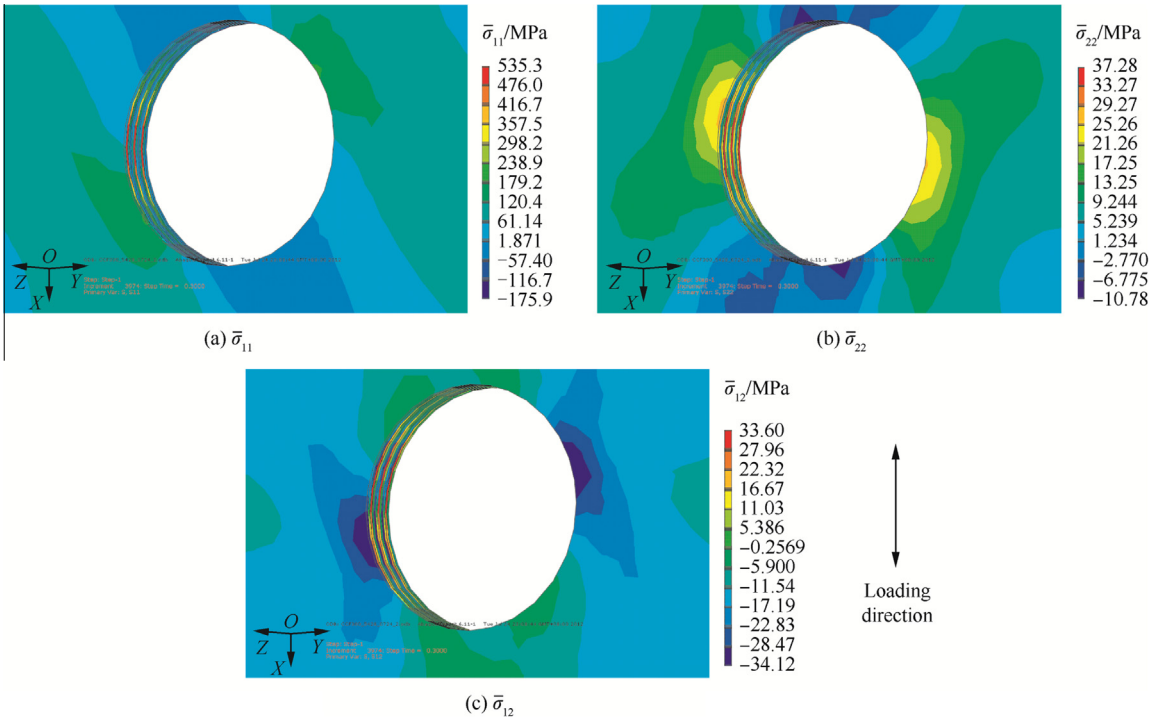

Fig. 15 State of stress at hole boundary before failure occurs.

results. The predicted strengths are a little lower than experimental results, which may be caused by the influence of inter-laminar stresses. It can be seen that the stress–strain curves before final failure caused by fiber breakage are quite straight, which means matrix damage does not apparently reduce the stiffness of the laminate. The slopes of CCF300/5228 and CCF300/5428 are nearly the same, while T700/5428 has a lower slope, which is caused by the different tensile modulus of CCF300 and T700 fibers. All the three curves drop abruptly when final failure occurs. Besides, the experimental curve of T700/5428 shows a small descent in the vicinity of ultimate strength which may be caused by some delamination, but this does not greatly influence the ultimate strength of the laminate.

Fig. 15 shows the state of stress at the hole boundary before any failure occurs. It can be seen that in longitudinal stress ($\bar{\sigma}_{11}$) distribution, 0° plies have the maximum stress, where fiber tensile failure is most likely to initiate. In transverse stress ($\bar{\sigma}_{22}$) distribution, 90° plies and ±45° plies all have relatively high stress values, where matrix dilatational failure is most likely to occur, since $\bar{\sigma}_{22}$ contributes most to the first stress invariant I_1 of the matrix. In in-plane shear stress ($\bar{\sigma}_{12}$) distribution, ±45° plies have relatively high stress; $\bar{\sigma}_{12}$ contributes most to the von Mises equivalent stress σ_{VM} so matrix distortional failure is most likely to occur. The predicted damage patterns immediately after final failure agree well with observed experimental failure patterns as shown in Fig. 16. From this we can see that in all of the three materials, 0° plies have the most fiber breakage failure, 90° plies and ±45° plies have extensive matrix dilatational failure, while ±45° plies have the most matrix distortional failure. This also accords with the stress state at the hole boundary shown in Fig. 15.

Meanwhile, there are obvious different failure behaviors between three material systems, which is consistent with experimental results. CCF300/5228 laminate has a brittle failure pattern, in which matrix dilatation and distortion failure occurs in a limited zone on both sides of the hole, perpendicular to the loading direction. Fiber tensile failures traverse 0° and ±45° plies, while in 90° plies there is little fiber compressive failure near the hole caused by Poisson's effect. In contrast to CCF300/5228, CCF300/5428 has almost the same fiber strength but lower matrix strength, whose damage patterns are quite different. There is much more severe matrix dilatation and distortion damages before final failure in all plies, especially the matrix distortion damage of 0° plies in the vicinity of the hole which effectively relieves the stress concentration. In ±45° plies the contours of matrix failure are quite parallel with the fiber direction, which to some extent replaces fiber breakage at the final failure. T700/5428 has a much higher fiber tensile strength and the same matrix type as CCF300/5428, and its high strength of OHT laminate is mainly attributed to the fiber. There is extensive matrix dilatational and distortional failure in ±45° and 90° plies, while fiber tensile failure only occurs in 0° plies. In all of the three simulated damage patterns, each type of damage is slightly more severe in inner plies than outer plies, which is caused by the plane strain effects in inner plies. The numerically predicted results demonstrate that this new multi-scale failure criterion can effectively be used in the analysis of failure behavior of different matchings of fibers and matrix materials.

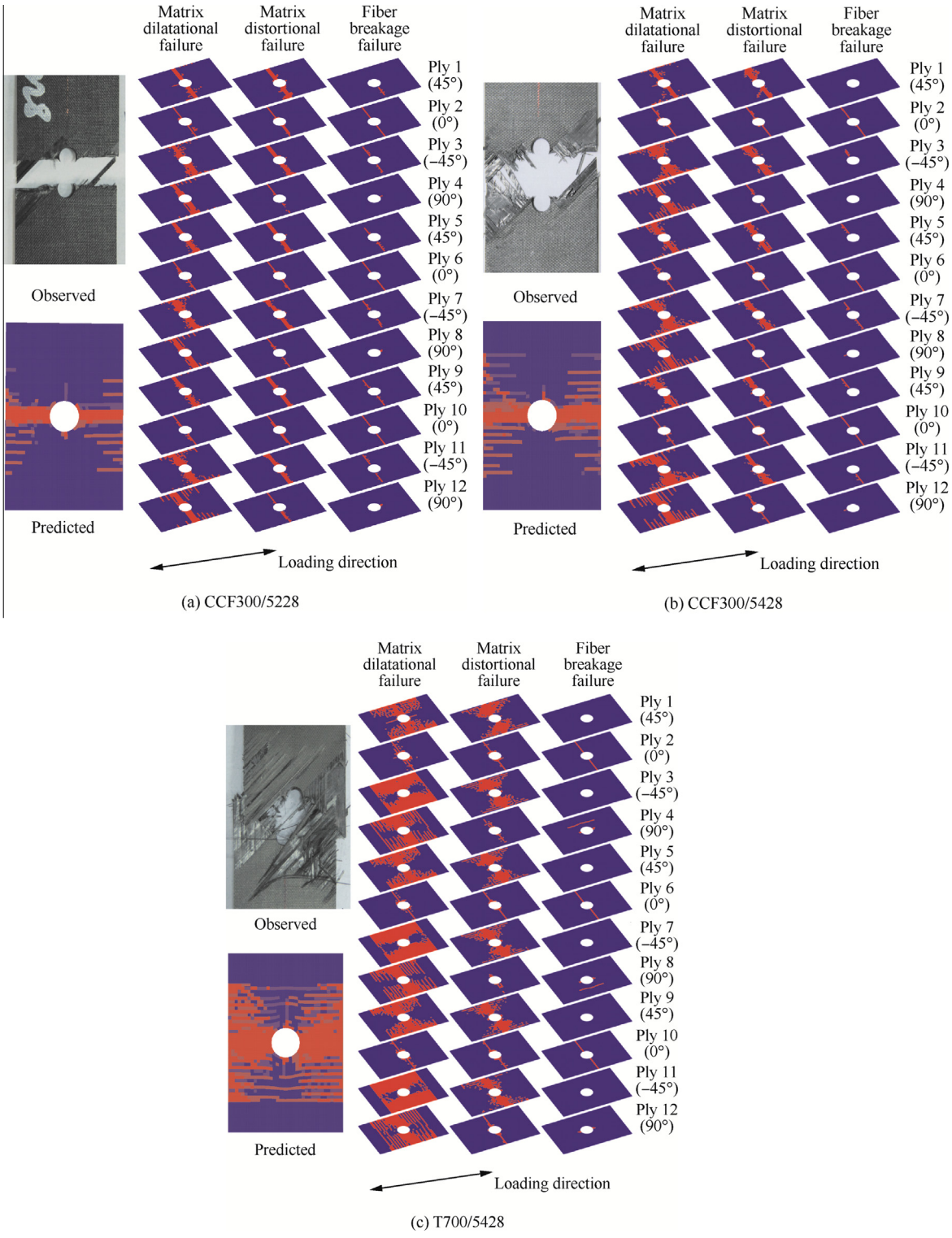

Fig. 16 Predicted damage patterns of three types of OHT specimen.

5. Conclusions

(1) The newly proposed multi-scale failure criterion achieves the whole processes of damage identification, determination and evolution, which helps to further understand the failure mechanism of composites.

(2) OHT tests conducted in three composite systems with various combinations of fiber and matrix show distinctively different failure manners. The ultimate strength and failure patterns of OHT specimens predicted by the multi-scale failure criterion are in good agreement with those from experiments.

(3) The modulus of fiber and matrix as well as their relative strengths result in different failure modes of composite laminates. Matrix damage prior to final failure alleviates the stress concentration in 0° ply, which effectively raises the ultimate strength of the laminate, while fiber strength is a key issue in the strength of the composites.

Acknowledgement

The authors would like to thank the National Basic Research and Development Program of China: Basic Scientific Research of Advanced Composites in Aeronautic and Astronautic Application Technology (No. 2010CB631103).

References

1. Karal M. *AST composite wing program – executive summary*. Long Beach (CA): The Boeing Company; 2001.
2. Du SY, Guan ZD. Strategic considerations for development of advanced composite technology for large commercial aircraft in China. *Acta Mater Compos Sin* 2008;**25**:1–10 Chinese.
3. Orifici A, Herszberg I, Thomson R. Review of methodologies for composite material modelling incorporating failure. *Compos Struct* 2008;**86**:194–210.
4. Tsai SW, Wu EM. A general theory of strength for anisotropic materials. *J Compos Mater* 1971;**5**:58–80.
5. Hashin Z. Failure criteria for unidirectional fiber composites. *J Appl Mech* 1980;**47**:329–34.
6. Hinton MJ, Kaddour AS, Soden PD. Failure criteria in fibre reinforced-polymer composites. *The world-wide failure exercise*. UK: Elsevier Ltd.; 2004.
7. Totry E, Molina-Aldareguía JM, González C, Lorca J. Effect of fiber, matrix and interface properties on the in-plane shear deformation of carbon-fiber reinforced composites. *Compos Sci Technol* 2010;**70**:970–80.
8. Hahn GL. *Accelerated insertion of materials-composites (AIM-C) methodology*. Chicago: Boeing Phantom Works, The Boeing Company; 2004.
9. Gosse JH, Christensen S. Strain invariant failure criteria for polymers in composite materials. *42nd AIAA/ASME/ASCE/AHS/ASC structures, structural dynamics, and materials conference and exhibit technical papers*; Seattle (WA). 2001. p. 45–55.
10. Mayes JS, Hansen AC. A comparison of multicontinuum theory based failure simulation with experimental results. *Compos Sci Technol* 2004;**64**:517–27.
11. Mayes JS, Hansen AC. Composite laminate failure analysis using multicontinuum theory. *Compos Sci Technol* 2004;**64**:379–94.
12. Wang CH. Progressive multi-scale modelling of composite laminates. In: Soutis C, Beaumont PWR, editors. *Multi-scale modelling of composite material systems: the art of predictive damage modelling*. Cambridge, England: Woodhead Publishing in Materials; 2005. p. 259–77.
13. Ha SK, Jin KK, Huang YC. Micro-mechanics of failure (MMF) for continuous fiber reinforced composites. *J Compos Mater* 2008;**42**:1873–95.
14. Ha SK, Huang YC, Han HH, Jin KK. Micromechanics of failure for ultimate strength predictions of composite laminates. *J Compos Mater* 2010;**44**:2347–61.
15. Pineda EJ, Waas AM, Bednarcyk BA, Collier CS, Yarrington PW. *A novel multiscale physics based progressive failure methodology for laminated composite structures*. Report No.: NASA/TM-2008-215448. Washington, D.C.: NASA; 2008.
16. Arnold SM, Bednarcyk BA, Hussain A, Kativar V. *Micromechanics-based structural analysis (FEAMAC) and multiscale visualization within Abaqus/CAE environment*. Report No.: NASA/TM-2010-216336. Washington, D.C.: NASA; 2010.
17. Gotsis PK, Chamis CC, Minnetyan L. Prediction of composite laminate fracture: micromechanics and progressive fracture. *Compos Sci Technol* 1998;**58**:1137–49.
18. Huang Z. A bridging model prediction of the ultimate strength of composite laminates subjected to biaxial loads. *Compos Sci Technol* 2004;**64**:395–448.
19. Li R, Kelly D, Crosky A. An evaluation of failure criteria for matrix induced failure in composite materials. *Compos Struct* 2002;**57**:385–91.
20. Tay TE, Tan SHN, Tan VBC, Gosse JH. Damage progression by the element-failure method (EFM) and strain invariant failure theory (SIFT). *Compos Sci Technol* 2005;**65**:935–44.
21. Sun XS, Tan VBC, Tay TE. Micromechanics-based progressive failure analysis of fibre-reinforced composites with non-iterative element-failure method. *Comput Struct* 2011;**89**:1103–16.
22. Tay TE, Liu G, Tan VBC, Sun XS, Pham DC. Progressive failure analysis of composites. *J Compos Mater* 2008;**42**:1921–66.
23. Jasso AJM, Goodsell JE, Ritchey AJ, Pipes RB, Koslowski M. A parametric study of fiber volume fraction distribution on the failure initiation location in open hole off-axis tensile specimen. *Compos Sci Technol* 2011;**71**(16):1819–25.
24. Mayes JS, Key CT, Six RW, Nickerson S. *A thermal–mechanical failure analysis of composites at cryogenic temperatures using multi-continuum theory*. Laramie (WY): Firehole Technologies; 2003.
25. Cai H, Miyano Y, Nakada M. Long-term open-hole compression strength of CFRP laminates based on strain invariant failure theory. *J Thermoplast Compos* 2009;**22**:63–81.
26. Ye L, Afaghi-Khatibi A, Lawcock G, Mai Y. Effect of fibre/matrix adhesion on residual strength of notched composite laminates. *Compos A Appl Sci Manuf* 1998;**29**:1525–33.
27. Hoecker F, Friedrich K, Blumberg H, Karger-Kocsis J. Effects of fiber/matrix adhesion on off-axis mechanical response in carbon-fiber/epoxyresin composites. *Compos Sci Technol* 1995;**54**:317–27.
28. Deng S, Ye L. Influence of fiber–matrix adhesion on mechanical properties of graphite/epoxy composites: II. Interlaminar fracture and in plane shear behavior. *J Reinf Plast Compos* 1999;**18**:1041–57.
29. Koyanagi J, Yoneyama S, Nemoto A, Melo JDD. Time and temperature dependence of carbon/epoxy interface strength. *Compos Sci Technol* 2010;**70**:1395–400.
30. Raghasva R, Caddell RM, Yeh GS. The macroscopic yield behaviour of polymers. *J Mater Sci* 1973;**8**:225–32.
31. Asp LE, Berglund LA, Talreja R. A criterion for crack initiation in glassy polymers subjected to a composite-like stress state. *Compos Sci Technol* 1996;**56**:1291–301.
32. Yudhanto A. Effects of micromechanical factors in the strain invariant failure theory for composites [dissertation]. Singapore: National University of Singapore; 2005.
33. Chamis C, Sinclair J. Ten-deg off-axis test for shear properties in fiber composites. *Exp Mech* 1977;**17**:339–46.
34. ASTM D 5766/D 5766M – 02a. Standard test method for open hole tensile strength of polymer matrix composite laminates. *Annual Book of ASTM Standards*. West Conshohocken (PA): ASTM; 2002.
35. Chen XB. *Handbook of polymer matrix composite materials*. Beijing: Chemical Industry Press; 2004.
36. Li H, Dai F, Du S. Numerical and experimental study on morphing bi-stable composite laminates actuated by a heating method. *Compos Sci Technol* 2012;**72**:1767–73.

Li Xing is a Ph.D. student at School of Aeronautic Science and Engineering, Beihang University. His area of research includes composite structures design and composite damage simulation.

Guan Zhidong is a professor and Ph.D. supervisor at School of Aeronautic Science and Engineering, Beihang University. His current research interests are composite damage tolerance, composite repair and composite design.